Research Article | Vol. 29, No. 8 / 12 April 2021 / Optics Express 12195
Optics EXPRESS

Polymer-coated quartz tuning fork for enhancing the sensitivity of laser-induced thermoelastic spectroscopy

CUNGUANG LOU,[1,2] XITONG LI,[1] HONGJIA CHEN,[1] XU YANG,[1] YU ZHANG,[1] JIANQUAN YAO,[2,3] AND XIULING LIU[1,4]

[1]College of Electronic Information Engineering & Hebei Key Laboratory of Digital Medical Engineering, Hebei University, Baoding 071002, China
[2]College of Precision Instrument and Optoelectronics Engineering, Institute of Laser and Optoelectronics, Tianjin University, Tianjin 300072, China
[3]jqyao@tju.edu.cn
[4]liuxiuling121@hotmail.com

Abstract: A novel laser-induced thermoelastic spectroscopy (LITES) sensor based on a polymer-coated quartz tuning fork (QTF) is reported. Two types of polymer films with different thicknesses are deposited on commercially available QTF to improve the conversion efficiency of laser energy deposition into vibration. CO_2 was selected as the target analyte for validation measurements. The experimental results indicate that by introducing a polymer coating, a maximum gain factor of 3.46 and 3.21 is attained for the signal amplitude and signal-to-noise ratio (SNR), respectively, when compared to traditional LITES that using only a bare QTF. A minimum detectable concentration of 0.181% can be obtained, corresponding to a normalized noise equivalent absorption coefficient (NNEA) of 1.74×10^{-11} $cm^{-1}\cdot W\cdot Hz^{-1/2}$, and the measurement precision is approximately 0.06% with an averaging time of 200 s. Here, we show what we believe is the first demonstration of polymer coated QTF for LITES sensing, compared with custom QTF, the design has the virtues of lower cost, simple and easy-to-operate, is a promising new strategy for sensitive trace gas analysis.

1. Introduction

Sensitive and selective detection of trace gases is critical in monitoring the atmospheric environment and investigating health status of the human body. A variety of gas molecular detection techniques have been studied extensively, including electronic noses, mass spectrometry and optical fiber sensing [1–3]. As an important sensing technique, laser absorption spectroscopy provides the advantages of high sensitivity, high specificity and fast response. One of the most sensitive optical gas sensing techniques is tunable diode laser absorption spectroscopy (TDLAS), which has been commonly employed for the measurements of trace gases, such as methane and ammonia [4–5]. Quartz-enhanced photoacoustic spectroscopy (QEPAS) is another ultrahigh sensitive gas sensing technique that employs the detection of sound waves arising from the gas absorption to modulated light [6–11]. One of the main advantages of QEPAS is that no photodetector is required as it is replaced by a quartz tuning fork (QTF) with a high-quality factor (Q). However, QEPAS is not suitable for the detection of corrosive gases as they can compromise the QTF resonance properties [12,13].

The QTF sensor has the benefits of low cost and compact size, and the narrow resonance frequency response of QTF results in a high signal-to-noise ratio (SNR), QTFs have been demonstrated to sensitive to electromagnetic radiation ranging from the near-infrared to terahertz frequency [14–17]. Most recently, quartz-enhanced photothermal spectroscopy (QEPTS), also called light-induced thermoelastic spectroscopy (LITES) was developed to overcome the above

#421356 https://doi.org/10.1364/OE.421356
Journal © 2021 Received 2 Feb 2021; revised 26 Mar 2021; accepted 26 Mar 2021; published 5 Apr 2021

Optics EXPRESS

limitations of QEPAS technique. When a laser pulse is irradiated on the surface of the QTF, thermal energy is deposited due to light absorption, inducing an instantaneous temperature rise and a mechanical motion of tuning fork arms by thermoelastic conversion [18]. Ma et al. first employed the LITES to detect C_2H_2, achieving an improved performance compared with conventional TDLAS and QEPAS [19]. He et al. developed ultra-high sensitive LITES based on QTF and a 10 m-Herriot cell, achieved a CO minimum detection limit (MDL) of 17 ppb [20]. Zhang et al. proposed a QTF self-difference technique by illuminating two laser beams on opposite sides of one tuning fork arm, achieving a 5.1 times improvement in the SNR [21]. Hu et al. developed quartz-enhanced photoacoustic-photothermal spectroscopy (QEPA-PTS) by adding the photoacoustic and photothermal signals generated from two QTFs, a several times gain in the signal level was achieved [22].

The performance of a QTF-based LITES sensor is related to the thermal, mechanical and optical properties of the cantilever materials. The metal film deposited on the surface of QTF results in high light reflectivity, modifying the surface coating has been demonstrated to be a promising approach to improve the QTF sensitivity [23]. Ma et al. remove the metal films to improve the laser absorption [24], Kwon et al. presented cantilevers modified with a layer of black silicon nanocone arrays that were twice as responsive to infrared (IR) radiation [25]. Inada et al. coated cantilevers with colloidal graphite as a photothermal conversion layer to improve the photothermal excitation efficiency [26]. Recently, Zhou et al. coated two-dimensional Fe-doped cobaltous oxide on the QTF to enhance the photothermal effect [27]. The vibration amplitude of a QTF is directly related to the difference in thermal expansion coefficient between the silicon or silicon nitride (SiN_x) substrate and the surface-coating material. Employing material with a large thermal expansion coefficient can therefore further improve its sensitivity.

In this study, we report a polymer-coated QTF as a photodetector for the detection of infrared light. In combination with a long path length gas cell and wavelength modulation spectroscopy, a novel high sensitive LITES system was developed for gases detection. Two different types of polymer materials were selected and coated on to the QTF surface with different thickness. The 2f signal amplitude and SNR were recorded and compared with the QTF without coating. Carbon dioxide (CO_2) was chosen as the gas analyte to validate the system performance and the Allan variance was measured for statistical analysis.

2. Theory and design optimization

When the tuning fork prongs or cantilever receives radiation from an intensity modulated laser with incident power P, the temperature rise (ΔT) within the heated region is directly related to the irradiation power and thermodynamic parameters of QTF, which is given by the heat equation:

$$\rho C_p \frac{dT}{dt} = \frac{Q(t)}{V} - \lambda \nabla^2 T, \tag{1}$$

where Q(t), ρ, C_p, V and λ are the absorbed power, density, heat capacity, heated volume and effective thermal conductivity, respectively. Thermal diffusion leads to a temperature gradient, and the thermal expansion mismatch of the cantilever's two layers resulting in the deflection, the vibration amplitude (δ) at the tip can be found from the equation [21,28]:

$$\delta = 2(\beta_1 - \beta_2)\frac{d_1 + d_2}{{d_2}^2 K}\frac{L^3}{(\lambda_1 d_1 + \lambda_2 d_2)w} P\mu_a, \tag{2}$$

where

$$K = 4 + 6\frac{d_1}{d_2} + 4\left(\frac{d_1}{d_2}\right)^2 + \frac{E_1}{E_2}\left(\frac{d_1}{d_2}\right)^3 + \frac{E_2 d_2}{E_1 d_1}, \tag{3}$$

Here, L is the length of the cantilever, w is its width, d is the layer thickness, μ_a is the light absorption coefficient, β is the thermal expansion coefficient, and E is the elastic modulus. The

Optics EXPRESS

subscripts 1 and 2 correspond to the thin coating layer on the surface of cantilever and the substrate material, respectively. The sensitivity of the QTF sensor, $S=\delta/P\mu_a$, can be obtained from Eq. (2) and Eq. (3) and written as [29]:

$$S = 2\frac{\beta_2}{\lambda_2}\frac{L^3}{{d_2}^2 w}\theta, \quad \text{where} \quad \theta = \frac{(\phi - 1)(n + 1)}{K(\gamma n + 1)} \tag{4}$$

here $\gamma=\lambda_1/\lambda_2$, $\phi=\beta_1/\beta_2$, $n = d_1/d_2$. The sensitivity consists of thermal properties of substrate material and geometrical parameters, and the second term θ contains the ratios of the geometrical and the thermal properties of the two layers. It is clear that θ increases when ϕ is increased and γ is decreased. For the purpose of maximizing S, it is perhaps best to choose a few coating materials with large value of β and small value of λ. Generally, the Cr, Au, Al or Ag metallic layer was coated on the surface of the commercial tuning fork, one simple and practicable strategy to increase the sensitivity is coating another layer on the surface with high thermal expansion and low thermal diffusion materials.

When an additional layer was coated on the surface of commercially available QTF, tri-layer structure cantilever was formed, the sensitivity in Eq. (4) can be written as [30,31]:

$$S = \frac{6((\beta_2 - \beta_1)M_1 + (\beta_3 - \beta_2)M_2)}{6(d_1 + d_2)(d_2 + d_3) + M_3 + 3M_4}, \tag{5}$$

$$\begin{cases} M_1 = \left(1 + \dfrac{E_2 d_2}{E_3 d_3}\right)(d_1 + d_2) + (d_2 + d_3) \\ M_2 = \left(1 + \dfrac{E_2 d_2}{E_1 d_1}\right)(d_2 + d_3) + (d_1 + d_2) \\ M_3 = \dfrac{E_1 d_1 + E_2 d_2 + E_3 d_3}{E_1 d_1 E_3 d_3}(E_1 {d_1}^3 + E_2 {d_2}^3 + E_3 {d_3}^3) \\ M_4 = \left(1 + \dfrac{E_2 d_2}{E_3 d_3}\right)(d_1 + d_2)^2 + \left(1 + \dfrac{E_2 d_2}{E_1 d_1}\right)(d_2 + d_3)^2 \end{cases} \tag{6}$$

Here, the subscripts 1, 2 and 3 correspond to the substrate material, metallic coating layer and the additional coating layer on the surface of cantilever, respectively. As can be seen from the equation, large thermal expansion mismatch leading to the bend of the cantilever, and hence much higher sensitivity can be obtained by employing suitable coating material. The polymer was selected due to its large thermal expansion coefficients, for example polydimethylsiloxane (PDMS), whose value ($960\times10^{-6}\cdot K^{-1}$) is 50.5 times larger than that of silver ($19\times10^{-6}\cdot K^{-1}$). Two kinds of polymer compounds were selected for the study, Polyimide (PI) and PDMS. Since the QTF is composed of a SiN_x substrate and a thin layer of silver, Table 1 lists some parameters of the silicon nitride substrate, silver and polymer materials, such as thermal conductivity, thermal expansion coefficient, specific heat capacity and elastic modulus.

Table 1. Property of materials used in simulation and experiment[abc]

Materials	λ ($W\cdot m^{-1}\cdot K^{-1}$)	β ($\times10^{-6}K^{-1}$)	C_p ($J\cdot kg^{-1}\cdot K^{-1}$)	E (GN/m^2)
Silicon Nitride	32	0.8	703	180
Silver	428	19	235	83
PI	0.1-0.35	20-30	1090	2.914
PDMS	0.18	960	1460	$1\text{-}10\times10^{-3}$

[a]From J. App. Phys. 104(5), 647-581 (2008).
[b]From Opt. Express. 21(11), 13256-13271 (2013).
[c]From Nat. Photonics. 8(7), 537-542 (2014).

Optics EXPRESS

The sensitivity obtained from Eq. (4) and Eq. (5) was performed with Matlab simulation and the results were shown in Fig. 1. As depicted in Fig. 1(a), layers 1 and 2 correspond to SiN_x and Ag respectively and layer 3 is the coating layer, a higher β value leads to higher vibration amplitude of the tuning fork prongs. When the coating material has a β value of $960\times10^{-6}\cdot K^{-1}$, the vibration amplitude is about 22 times higher than that applying an coating material with a β value of $19\times10^{-6}\cdot K^{-1}$, when the other parameters are unaltered. Figure 1(b) displays the simulation results of the vibration amplitude as a function of coating thickness and thermal parameters of the coating materials. It can be seen that the largest amplitude is achieved with large thermal expansion coefficient materials. Moreover, the vibration amplitude first increases and then decreases with increasing layer thickness with an optimal coating thickness. When the coating material has a similar β value with the metallic layer, the coating layer has only a limited impact on the thermal expansion mismatch, the amplitude decreases with increasing coating thickness immediately, due to coating affects the Q value. In this study, the detection sensitivity was optimized by varying the coating thickness and verified by experimental measurement.

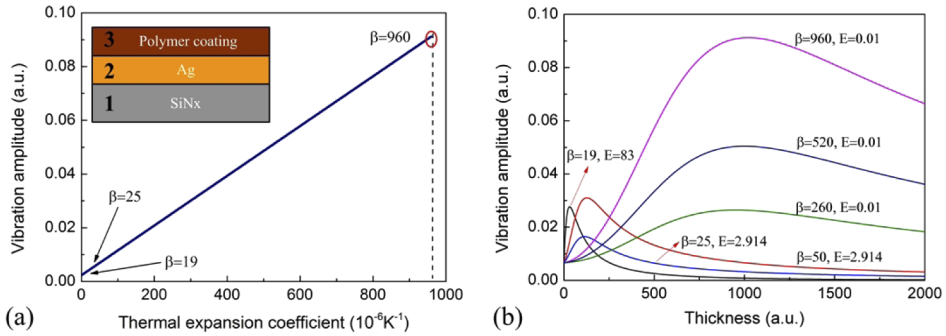

Fig. 1. (a) Simulated vibration amplitude of QTF as a function of coating layers thermal expansion coefficient. (b) Simulation results of the vibration amplitude as a function of coating thickness and thermal parameters of the coating materials.

3. Experimental details

A schematic diagram of the improved polymer-coated LITES sensor for gas detection is shown in Fig. 2(a). A fiber-coupled distributed feedback laser diode (PL-DFB-1580-B1-SA-14BF) operating at 1580.51 nm with a maximum laser power of 25 mW was selected as the wavelength scanning laser source. The wavelength of the DFB laser is modulated by adjusting the injection current and the operating temperature. The driving current was regulated by using a laser diode controller (Thorlabs, LDC202C) and the laser temperature was set to 16 °C using a temperature control module (KW_DFB). The driving signal is the superposition of sinusoidal and sawtooth signals generated by a dual-channel function generator (Tektronix AFG3022C). The laser beam collimation and contraction were first carried out, and then the parallel light beam entered into the Herriott cell.

A commercially available quartz crystal oscillator with a removed shell was used as the QTF detector, the nominal resonance frequency was 32,768 Hz. The output laser beam from the gas cell was focused by a CaF_2 lens with a focal length of 40 mm (Thorlabs, LA1304-C), then radiated on the root of one QTF prong and excited thermoelastic signal. The focal point position is shown in Fig. 2(b). A photograph of the device used is shown in Fig. 2(c) and the signal amplifier circuit of QTF is shown in Fig. 2(d). The piezoelectric-current of the QTF was first amplified by a self-made trans-impedance amplifier (AD712JR) with a 22 MΩ feedback resister and 3 MHz bandwidth. The harmonic signal was then demodulated by a lock-in amplifier

Optics EXPRESS

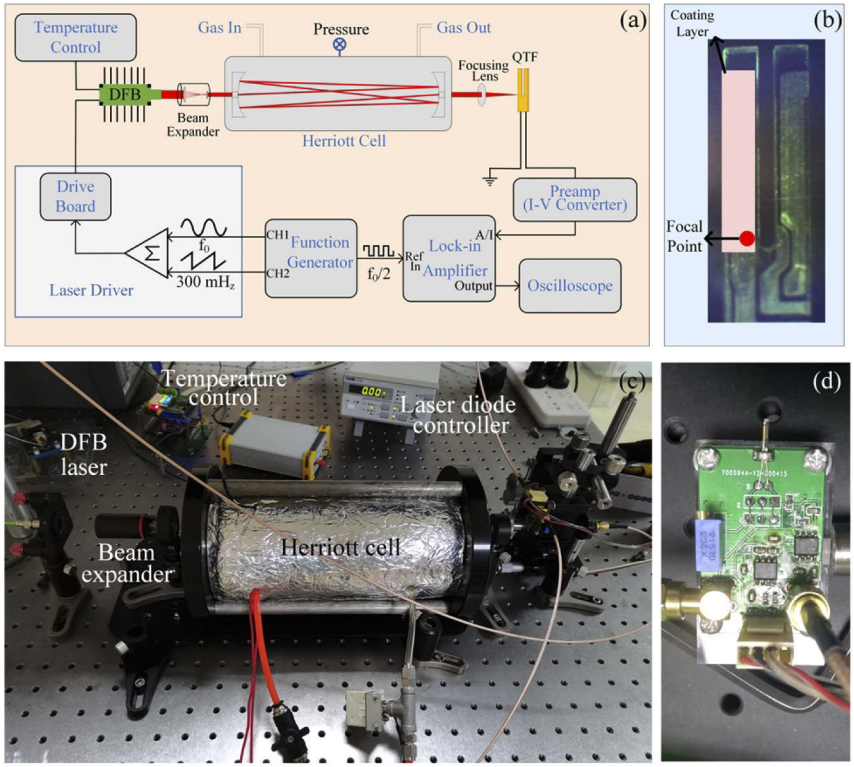

Fig. 2. (a) Schematic diagram of the LITES gas detection system. (b) The focal point of the laser beam on the QTF and the location of the polymer coating. (c) Photograph of the device used. (d) Photograph of the QTF signal adjustment circuit.

(SYSU, Sine Scientific Instruments, OE2031) and finally digitized by an oscilloscope (Tektronix MDO3012). Throughout the experiment, the lock-in amplifier sensitivity was set at 5 mV to ensure the consistent signal gain. The filter slope was set to 24 dB/oct and a time constant of 100 ms, and thus the detection bandwidth was calculated to be 1.10 Hz.

The strong CO_2 absorption line at 1580.51 nm was selected as the target line. The absorption line intensity is 1.3×10^{-23} $cm^{-1}/(mol\cdot cm^{-2})$ according to the HITRAN and SpectraPlot database [32,33]. A direct ramp current drives the DFB laser diode to tune the emission wavelength, scanning across the target absorption line at 6327 cm^{-1}. The modulation frequency of sinusoidal voltage is half of the resonance frequency of the QTF. The second harmonic (2f) signal was extracted for concentration measurements. Pure N_2 was first introduced into the gas cell to remove residual gas. Then, a mixture of CO_2 and N_2 at different concentrations was introduced into the gas cell at a pressure of 1.5 kPa.

4. Results and discussions

The performance of the QTF-based LITES sensor was experimentally investigated to verify the correct selection of the CO_2 absorption lines. Figure 3(a) shows the absorption spectrum captured from the HITRAN database [32]. The absorption line marked with a red dotted line was selected as the target. The concentration of CO_2 used for the first measurement was 6%, and a typical raw absorption signal around 6327 cm^{-1} and the demodulated 2f signal are shown in Fig. 3(b). A ramp wave from 35 mA to 85 mA allows retrieving a complete profile of one target absorption line, a distinct sawtooth waveform depression was obtained in the blue line indicating

Optics EXPRESS

a significant absorption of CO_2 at this wavelength. The red line corresponds to the 2f signal obtained by the bare QTF with an amplitude of about 32 mV and a SNR of 9.96.

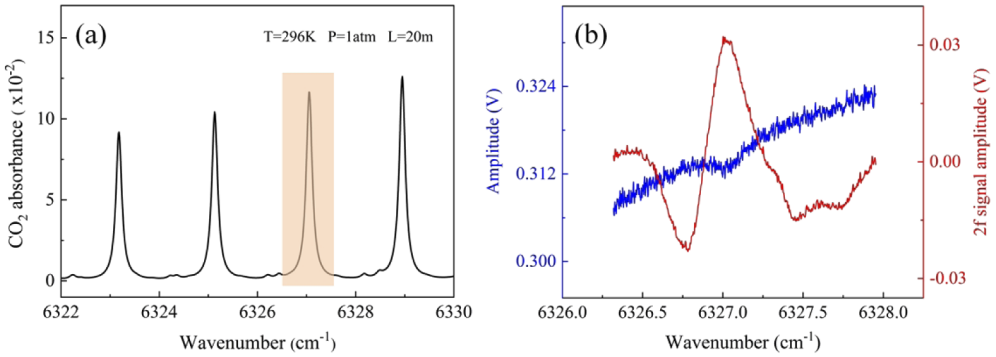

Fig. 3. (a) The CO_2 absorption lines at around 1580 nm. (b) The CO_2 absorption signal with a 6% concentration detected by the photodetector (DET08CL/M) and the 2f signal demodulated from the QTF detector.

Polyimide was the first polymer investigated for the coating layer. It is not easily dissolved in most organic solvents, so *N*-methyl pyrrolidone (NMP) was selected as the solvent in a 1:1 ratio. The dissolved solution is coated on the tuning fork arm and heated 15 min at a temperature of 150 °C. In this group of experiments, the QTFs were spin-coated with PI of different thicknesses and numbered as #1, #2, #3, #4 and #5, according to the coating thickness. A higher coating thickness corresponds to a thicker polymer compound. An uncoated tuning fork (Bare) was used as a control, its signal amplitude was compared with the coated tuning fork to prove the effectiveness of coating.

A sinusoidal signal with an amplitude of 20 mV generated using a function generator was connected to the pins of the QTF driving it to vibrate at a frequency. Different response amplitude could be obtained by precisely adjusting the excitation signal frequency, with a maximum amplitude obtained at its resonance frequency. In the experiment, the sweep width of excitation signal was 100 Hz with a minimum step value of 0.01 Hz, and the amplitude-frequency response was collected by lock-in-amplifier with 3 ms time constant and 500 mV sensitivity. As shown in Fig. 4(a), the resonant frequencies of QTF with and without PI coating from bare to #5 are 32757, 32755, 32732, 32733, 32727 and 32731 Hz. The corresponding Q value from bare to #5 was calculated to be 6450.30, 5969.05, 5734.71, 5356.17, 6090.23 and 5753.43. According to the theoretical prediction, the resonant frequency of QTF is very sensitive to the mass loaded on the QTF arms. The observed changes in resonant frequency arise from the PI coating on the surface of the tuning fork.

Subsequently, CO_2 at a 6% concentration was introduced into the gas cell. The transmission laser was detected by the QTFs and demodulated by the lock-in amplifier, the 2f signal was obtained as displayed in Fig. 4(b). This figure shows that they have similar waveforms and slightly different amplitudes, the rise and fall of the waveforms show slight asymmetry which may arise from the optical interference. In addition, when the laser radiation intensity changes suddenly, the mechanical vibration of high quality tuning fork cannot response quickly, which might also cause a distortion in the tail of 2f signal. The noise for sensors employing bare QTF and PI-coated QTF was determined when the laser wavelength was adjusted away from the absorption peak of CO_2, as illustrated using dashed lines in Fig. 4(b). The measured noises for QTF with different coating thickness are shown in Fig. 4(c), by calculating the standard deviation we can found that the obtained noise amplitudes have no obvious increase, and the increase in noise value is less than 6% after coating.

Optics EXPRESS

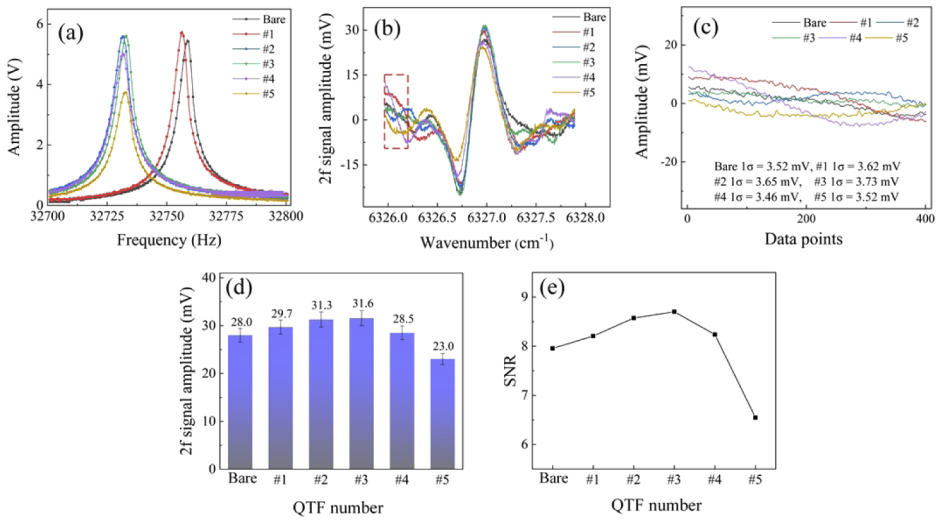

Fig. 4. (a) The QTF resonance curve with different PI coating thickness. (b) The 2f signal waveform of 6% CO_2 obtained by coating QTF with different thickness of PI. (c) Noise level determination. (d) The amplitude of 2f signals in figure (b). (e) The SNR of 2f signals in figure (b).

The amplitudes of 2f signals were extracted and shown in Fig. 4(d). There is an initial increase in the amplitudes followed by a subsequent decrease with the coating thickness. The QTF #3 has the largest value (31.6 mV), which is 1.129 times higher than that of the bare tuning fork (28.0 mV). Too thick coating films significantly increase the mass loading on the tuning fork arm, leading to a negative frequency shift and decrease in Q value, and hence the vibration amplitude under laser radiation decreases, consistent with theoretic predictions. The PI film thickness was measured by scanning electron microscopy (SEM), and the value for QTF #1 to #5 is around 370 nm, 460 nm, 540 nm, 650 nm and 730 nm, respectively. The SNR was calculated and is shown in Fig. 4(e). The SNR of QTF #3 is the largest (8.70), which is 1.09 times higher than that of the bare tuning fork (7.95). The above experimental data suggest that the PI coating increases the sensitivity to a certain extent. However, the improvement was not sufficient due to the similarity β value of PI to that of metal layer on the QTF surface.

Given the above results, we next investigated PDMS as a polymeric material for our sensor due to its large β value. The polymer PDMS and curing agent were mixed at a ratio of 10:1 and silicone oil was added as a diluent. The dissolved solution was spin coated on the tuning fork arm and heated at temperature of 70 °C for 2 h to solidify the polymer. Finally, the polymer coated QTF were numbered as #1, #2, #3, #4 and #5 according to the coating thickness. The resonance curve of these QTFs were measured firstly, as shown in Fig. 5(a), the experimental results show that the QTF resonant frequencies changes from 32750 Hz (bare) to 32733 (#1), 32733 (#2), 32753 (#3), 32753 (#4) and 32733 Hz (#5) after PDMS coating, with a Q value of 6409.12 (bare), 5866.13 (#1), 5752.81 (#2), 5233.82 (#3), 6550.71 (#4) and 5742.98 (#5). The 2f signals obtained by QTF with and without PDMS coating are shown in Fig. 5(b) and the signal amplitudes are given in Fig. 5(d). The noise for sensors employing bare QTF and PDMS-coated QTFs were determined and shown in Fig. 5(c). By calculating the standard deviation, the obtained noise amplitudes were around 3.5 mV, and the noise fluctuation is not greater than 7%, one can see that there is no obvious noise difference among these QTFs. As can be seen from the Fig. 5(d), the amplitude of the 2f signal detected by QTF #4 is the largest (106.7 mV), which is 3.46 times higher than that of the bare tuning fork (30.8 mV). Figure 5(e) indicates that the SNR of #4 is the

Optics EXPRESS

largest (29.32), which is 3.21 times higher than that of the bare tuning fork (9.15). The PDMS film thickness was measured by SEM, and the value for QTF #1 to #5 is around 430 nm, 560 nm, 670 nm, 750 nm and 830 nm, respectively.

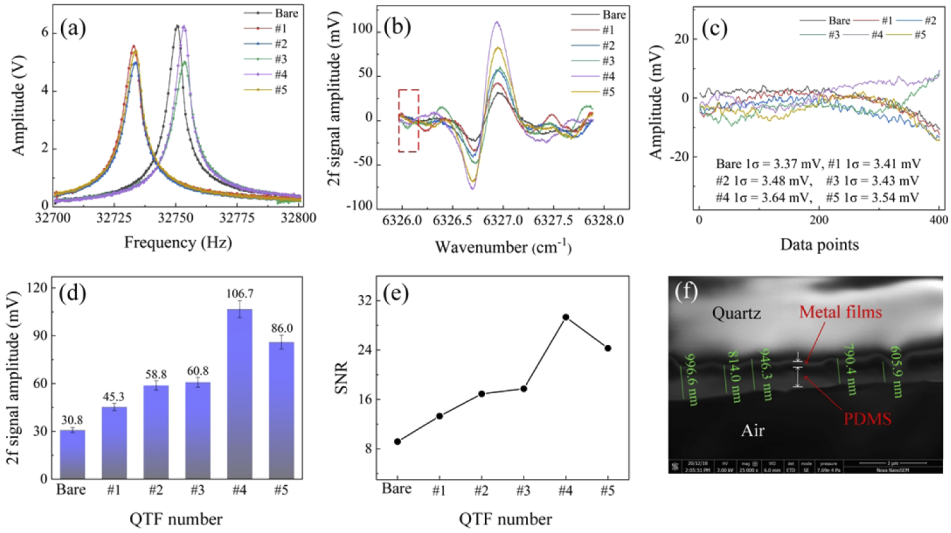

Fig. 5. (a) The resonance curve of QTF with different coating thickness of PDMS. (b) The 2f signal waveform of 6% CO_2 obtained by bare and PDMS-coated QTFs. (c) Noise level determination. (d) The amplitude of 2f signals in figure (b). (e) The SNR of 2f signals in figure (b). (f) SEM images of #4 PDMS-coated QTF.

Combining the above two groups of experiments, it can be concluded that there is only a 1.1 times increase of PI polymer layer, which caused by the relative small difference in β values of PI and Ag. However, both the amplitude and SNR of 2f signal increase significantly after PDMS coating, which is sufficient to demonstrate that PDMS can effectively improve the sensitivity of the LITES system by raising the thermal expansion coefficient mismatch of SiN_x substrate and surface layer. The #4 QTF was selected for the detection as it combines high sensitivity and high SNR. Stepwise concentration measurements of CO_2 from 10% down to 2.5% were performed to validate the linearity of the LITES signal as a function of concentration. For each concentration, 10 waveforms were collected and the 2f signal amplitudes were averaged to minimize random errors. Figure 6(a) presents typical 2f signals of pure N_2 and CO_2 at a concentration of 2.5%, 5%, 6%, 8% and 10%; the six plots show significant differences in amplitude. The SNR was calculated to be 33.22 for CO_2 at a 6% concentration indicating an MDL (1σ) of 0.181%. This yields a normalized noise equivalent absorption (NNEA) of 1.74×10^{-11} $cm^{-1}\cdot W\cdot Hz^{-1/2}$. It should be noted that the lock-in amplifier sensitivity was set at constant value to avoid signal saturation at high CO_2 concentration. The SNR can be further improved by increasing the signal gain of lock-in amplifier, thus higher sensitivity can be obtained. Figure 6(b) shows the 2f signal amplitude plotted at different CO_2 concentrations. It is clear that the fitting curves of 2f signal intensity increases as the gas concentration increases with a fitting coefficient R-value of 0.991, suggesting that the polymer-coated LITES sensor has an excellent linear response in the range measured.

Finally, the stability and precision of the LITES sensor system were investigated by continuous measurements at a 6% CO_2 concentration, the data sampling period was ~3 s, and the 2f signal amplitude was sampled and recorded for 2 h. Figure 7(a) shows 2,400 groups of 2f signal amplitude. The magnitude changes within the range of 0.08 to 0.12 V with a mean value of 0.1 V and a standard deviation of 5.97 mV, indicating the excellent stability of this system. Based on

Optics EXPRESS

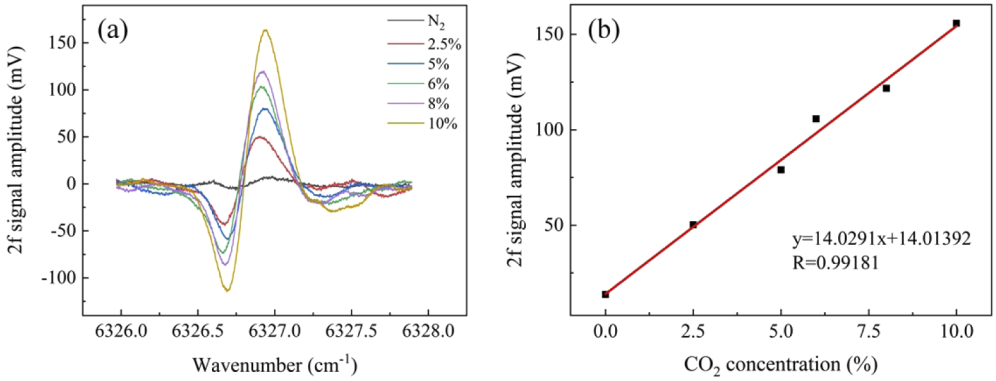

Fig. 6. (a) Experimentally measured 2f signals for N_2 and five different CO_2 concentrations. (b) The linear relationship between CO_2 concentration and 2f signal amplitude.

the gathered data, we calculated the Allan deviation as a function of averaging time, which is plotted in Fig. 7(b). As can be seen from the figure, when the averaging time increases to 200 s, a minimum value of the Allan deviation is reached, corresponding to a precision of approximately 0.06%. The QTF detector's amplitude response and SNR is linearly dependent on the incident laser power in a certain range, and thus the performance of the sensor system can be further improved by excitation power optimization [18]. Moreover, the Allan deviation indicates that the sensor system is mainly affected by the white noise and thus a higher sensitivity could be achieved using pulse modulated light.

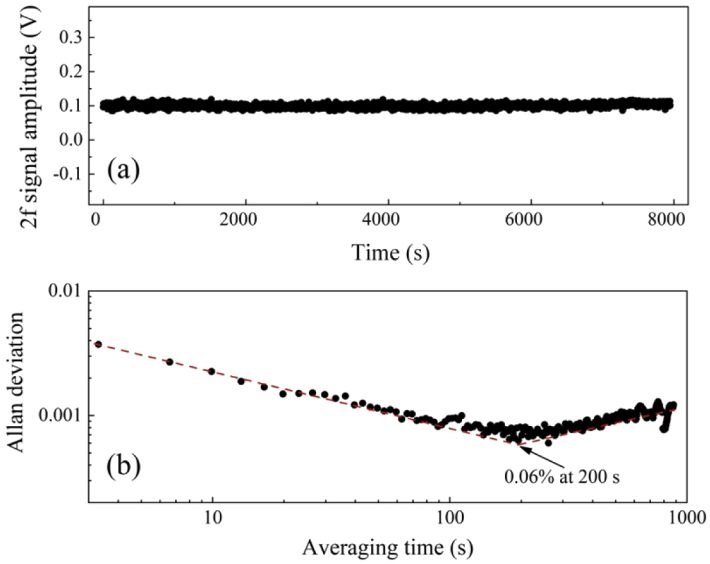

Fig. 7. (a) Long-term CO_2 measurements performed at a 6% concentration. (b) Allan deviation analysis of the PDMS-coated QTF-based LITES sensor.

The QTF-based LITES is an alternative approach to the QEPAS and TDLAS technique that could overcome some limitations and improve the gas sensor sensitivity [22]. The small laser spot diameter and optimal laser focusing position on the QTFs surface are essential for high sensitive detection. The extent of thermal deformation is proportional to the energy absorbed

Optics EXPRESS

by the cantilever, while the high reflectivity metallic film deposited on the surface of the QTF leading to a strong light scattering and thermal noise. The small optical absorbance is one of the limiting factors for improving sensitivity. Future research is warranted on coating the surface of QTF prongs with polymers of high light absorption to maximize the thermoelastic signal.

Moreover, the adhesion between the coating layer and the substrate affects the heat conduction and interlaminar stress gradient, hence the coating process needs to be further improved to transmit the absorbed laser energy and strain to the SiN_x substrate effectively, generate higher thermal deformation efficiency. In this work, a 1580 nm laser was employed for CO_2 detection, however, measurement of other trace gas analytes can be conducted by changing the excitation wavelength. Further improvement of the performance can be expected by packaging the QTF in a vacuum shell with an optical window instead of a tuning fork exposed to the air [34,35].

5. Conclusions

In summary, we have designed a novel polymer-coated LITES sensor by employing a standard commercially available QTF. The vibration characteristic of QTF prongs was optimized by coating polymer with high thermal expansion coefficient value. The sensitivity and SNR improvement was validated using CO_2 gas as the analyte, and a maximum gain factor of 3.46 times was achieved compared to traditional LITES. At the best-operating conditions, an MDL of 0.181% was achieved leading to an NNEA of 1.74×10^{-11} $cm^{-1}\cdot W\cdot Hz^{-1/2}$. The minimum value of Allan deviation reached to 0.06% when the averaging time is 200 s. This coating design is easy to operate and no special tuning fork design is required, and compared to the differential techniques using space optical systems, this design offers the advantage that it is less complex. The polymer-coated LITES sensor with improved sensitivity can be further exploited by coating with an absorption layer and it is a promising strategy for trace gas analysis.

Funding. Hebei province postdoctoral scientific research project (B2019005001); Hebei Provincial Key Research Projects (ZD2020146); Hebei Province Graduate Innovation Funding Project (HBU2021ss003).

Acknowledgments. The authors would like to thank all the colleagues that have supported this work.

Disclosures. The authors declare no conflicts of interest.

Data availability. Data underlying the results presented in this paper are not publicly available at this time but may be obtained from the authors upon reasonable request.

References

1. M. Nurjuliana, Y. B. C. Man, D. M. Hashim, and A. K. S. Mohamed, "Rapid identification of pork for halal authentication using the electronic nose and gas chromatography mass spectrometer with headspace analyzer," Meat Sci. **88**(4), 638–644 (2011).
2. V. V. Manoilov, L. V. Novikov, I. V. Zarutskii, A. G. Kuz'min, and Y. A. Titov, "Methods for Processing Mass Spectrometry Signals from Exhaled Gases for Medical Diagnosis," Biomed. Eng. **53**(5), 355–359 (2020).
3. Y. Z. Tan, W. Jin, F. Yang, Y. Qi, C. Z. Zhang, Y. C. Lin, and H. L. Ho, "Hollow-core fiber-based high finesse resonating cavity for high sensitivity gas detection," J. Lightwave Technol. **35**(14), 2887–2893 (2017).
4. L. Dong, F. K. Tittel, C. G. Li, N. P. Sanchez, H. P. Wu, C. T. Zheng, Y. J. Yu, A. Sampaolo, and R. J. Griffin, "Compact TDLAS based sensor design using interband cascade lasers for mid-IR trace gas sensing," Opt. Express **24**(6), A528–A535 (2016).
5. K. Owen and A. Farooq, "A calibration-free ammonia breath sensor using a quantum cascade laser with WMS 2f/1f," Appl. Phys. B **116**(2), 371–383 (2014).
6. S. Borri, P. Patimisco, A. Sampaolo, H. E. Beere, D. A. Ritchie, M. S. Vitiello, G. Scamarcio, and V. Spagnolo, "Terahertz quartz enhanced photo-acoustic sensor," Appl. Phys. Lett. **103**(2), 021105 (2013).
7. P. Patimisco, A. Sampaolo, M. Giglio, S. D. Russo, V. Mackowiak, H. Rossmadl, A. Cable, F. K. Tittel, and V. Spagnolo, "Tuning forks with optimized geometries for quartz-enhanced photoacoustic spectroscopy," Opt. Express **27**(2), 1401–1415 (2019).
8. S. D. Qiao, Y. F. Ma, P. Patimisco, A. Sampaolo, Y. He, Z. T. Lang, F. K. Tittel, and V. Spagnolo, "Multi-pass quartz-enhanced photoacoustic spectroscopy-based trace gas sensing," Opt. Lett. **46**(5), 977–980 (2021).
9. H. P. Wu, L. Dong, H. D. Zheng, Y. J. Yu, W. G. Ma, L. Zhang, W. B. Yin, L. T. Xiao, S. T. Jia, and F. K. Tittel, "Beat frequency quartz-enhanced photoacoustic spectroscopy for fast and calibration-free continuous trace-gas monitoring," Nat. Commun. **8**(1), 15331 (2017).

Optics EXPRESS

10. L. Dong, H. P. Wu, H. D. Zheng, Y. Y. Liu, X. L. Liu, W. Z. Jiang, L. Zhang, W. G. Ma, W. Ren, W. B. Yin, S. T. Jia, and F. K. Tittel, "Double acoustic microresonator quartz-enhanced photoacoustic spectroscopy," Opt. Lett. **39**(8), 2479–2482 (2014).
11. Y. He, Y. F. Ma, Y. Tong, X. Yu, and F. K. Tittel, "HCN ppt-level detection based on a QEPAS sensor with amplified laser and a miniaturized 3D-printed photoacoustic detection channel," Opt. Express **26**(8), 9666–9675 (2018).
12. H. M. Yi, R. Maamary, X. M. Gao, M. W. Sigrist, E. Fertein, and W. D. Chen, "Short-lived species detection of nitrous acid by external-cavity quantum cascade laser based quartz-enhanced photoacoustic absorption spectroscopy," Appl. Phys. Lett. **106**(10), 101109 (2015).
13. Y. F. Ma, Y. He, X. Yu, C. Chen, R. Sun, and F. K. Tittel, "HCl ppb-level detection based on QEPAS sensor using a low resonance frequency quartz tuning fork," Sens. Actuators, B **233**, 388–393 (2016).
14. L. G. Xu, N. W. Liu, S. Zhou, L. Zhang, B. L. Yu, H. Fischer, and J. S. Li, "Dual-frequency modulation quartz crystal tuning fork–enhanced laser spectroscopy," Opt. Express **28**(4), 5648–5657 (2020).
15. U. Willer, A. Pohlkötter, W. Schade, J. H. Xu, T. Losco, R. P. Green, A. Tredicucci, H. E. Beere, and D. A. Ritchie, "Resonant tuning fork detector for THz radiation," Opt. Express **17**(16), 14069–14074 (2009).
16. A. Pohlkötter, U. Willer, C. Bauer, and W. Schade, "Resonant tuning fork detector for electromagnetic radiation," Appl. Opt. **48**(4), B119–B125 (2009).
17. H. P. Wu, L. Dong, X. K. Yin, A. Sampaolo, P. Patimisco, W. G. Ma, L. Zhang, W. B. Yin, L. T. Xiao, V. Spagnolo, and S. T. Jia, "Atmospheric CH4 measurement near a landfill using an ICL-based QEPAS sensor with V-T relaxation self-calibration," Sens. Actuators, B **297**, 126753 (2019).
18. Y. F. Ma, Y. He, P. Patimisco, A. Sampaolo, S. D. Qiao, X. Yu, F. K. Tittel, and V. Spagnolo, "Ultra-high sensitive trace gas detection based on light-induced thermoelastic spectroscopy and a custom quartz tuning fork," Appl. Phys. Lett. **116**(1), 011103 (2020).
19. Y. F. Ma, Y. He, Y. Tong, X. Yu, and F. K. Tittel, "Quartz-tuning-fork enhanced photothermal spectroscopy for ultra-high sensitive trace gas detection," Opt. Express **26**(24), 32103–32110 (2018).
20. Y. He, Y. F. Ma, Y. Tong, X. Yu, and F. K. Tittel, "Ultra-high sensitive light-induced thermoelastic spectroscopy sensor with a high Q-factor quartz tuning fork and a multipass cell," Opt. Lett. **44**(8), 1904–1907 (2019).
21. Q. D. Zhang, J. Chang, Z. H. Cong, and Z. L. Wang, "Quartz tuning fork enhanced photothermal spectroscopy gas detection system with a novel QTF-self-difference technique," Sens. Actuators, A **299**, 111629 (2019).
22. Y. Q. Hu, S. D. Qiao, Y. He, Z. T. Lang, and Y. F. Ma, "Quartz-enhanced photoacoustic-photothermal spectroscopy for trace gas sensing," Opt. Express **29**(4), 5121–5127 (2021).
23. J. H. Ko, Y. W. Yoon, and J. C. Lee, "Quartz tuning forks with hydrogel patterned by dynamic mask lithography for humidity sensing," Sens. Actuators, B **273**, 821–825 (2018).
24. Y. F. Ma, Y. Q. Hu, S. D. Qiao, Y. He, and F. K. Tittel, "Trace gas sensing based on multi-quartz-enhanced photothermal spectroscopy," Photoacoustics **20**, 100206 (2020).
25. B. Kwon, J. Jiang, M. V. Schulmerich, Z. D. Xu, R. Bhargava, G. L. Liu, and W. P. King, "Bimaterial microcantilevers with black silicon nanocone arrays," Sens. Actuators, A **199**, 143–148 (2013).
26. N. Inada, H. Asakawa, T. Kobayashi, and T. Fukuma, "Efficiency improvement in the cantilever photothermal excitation method using a photothermal conversion layer," Beilstein J. Nanotechnol. **7**, 409–417 (2016).
27. S. Zhou, K. Chen, L. G. Xu, B. L. Yu, T. T. Jiang, and J. S. Li, "Ultrathin two-dimensional Fe-doped cobaltous oxide as a piezoelectric enhancement mechanism in quartz crystal tuning fork (QCTF) photodetectors," Opt. Lett. **46**(3), 496–499 (2021).
28. B. Kwon, M. Rosenberger, R. Bhargava, D. G. Cahill, and W. P. King, "Dynamic thermomechanical response of bimaterial microcantilevers to periodic heating by infrared radiation," Rev. Sci. Instrum. **83**(1), 015003 (2012).
29. J. Lai, T. Perazzo, Z. Shi, and A. Majumdar, "Optimization and performance of high-resolution micro-optomechanical thermal sensors," Sens. Actuators, A **58**(2), 113–119 (1997).
30. C. Lin and F. Fang, "Study on Dynamic Photothermal Mechanical Characteristics of Microcantilever with CNTs absorption Layer," Laser Journal **38**(1), 25–30 (2017).
31. L. B. Freund and S. Suresh, *Think film materials: stress, defect formation, and surface evolution[M]*. Cambridge University, (2003).
32. The HITRAN database can be found at http://www.hitran.com
33. https://www.spectraplot.com/absorption
34. Z. Q. Zhang, S. H. Jia, Y. L. Wang, Z. H. Tang, and F. Wang, "Research on the influence of transparent vacuum encapsulation quartz tuning fork on the photo-thermoelastic spectroscopy of acetylene," Mod. Phys. Lett. B **30**(30), 1650364 (2016).
35. S. Dello Russo, A. Zifarelli, P. Patimisco, A. Sampaolo, T. T. Wei, H. P. Wu, L. Dong, and V. Spagnolo, "Light-induced thermo-elastic effect in quartz tuning forks exploited as a photodetector in gas absorption spectroscopy," Opt. Express **28**(13), 19074–19084 (2020).